



ARTICLE



## Theoretical formula for the cosmic-ray muon attenuation coefficients of Pb, Cu, Zn, and Al

Rasha N. I. Altameemi <sup>a</sup>, Nurul Shazana Abdul Hamid <sup>a,b</sup>, Wan Mohd Aimran Wan Mohd Kamil <sup>a</sup> and Saad M. Saleh Ahmed <sup>c</sup>

<sup>a</sup>Department of Applied Physics, Faculty of Science and Technology, Universiti Kebangsaan Malaysia, UKM Bangi, Selangor, Malaysia;

<sup>b</sup>Space Science Centre (ANGKASA), Institute of Climate Change, Universiti Kebangsaan Malaysia, Bangi, Malaysia; <sup>c</sup>Department of Physics, College of Science, University of Baghdad, Baghdad, Iraq

### ABSTRACT

The attenuation coefficients of cosmic-ray muons through metal plates were theoretically determined. Three methods (A, B, and C) were proposed by the researchers using the experimental data of count rate which was obtained from the detection of cosmic-ray muons through metal plates of different thicknesses. Method A was applied to Pb, Cu, Zn, and Al, whereas Methods B and C were applied to Pb only. The proposed A and B methods were based on ignoring the detected count rate produced by the shower of electromagnetic cascades to obtain the attenuation of cosmic-ray muons. The values and the formula of the radiation length of metals were used in Method A to obtain a theoretical formula to measure the cosmic-ray muon attenuation coefficients. The results showed consistent behavior with the atomic number, mass number, and mass density. In Method C, the penetrating muon is assumed to generate many sources of photon-electron cascades at every collision. The result was successful in describing the theoretical count rate behavior and to implicitly determine the muon attenuation.

### ARTICLE HISTORY

Received 4 December 2019

Accepted 24 September 2020

### KEYWORDS

Cosmic-ray muon; metal absorber; muon attenuation coefficient; radiation length; shower effect

### 1. Introduction

Since cosmic-ray muon interaction with matter is a very interesting topic in explaining the muon shower in air, water, or in layers of metals, many theoretical treatments have been applied for interpretation by calculating the energy dissipation or stopping power ( $-\frac{dE}{dx}$ ) and cross-section (Stanev, 2010). The mean free path, the radiation length, and the attenuation or absorption coefficient are significant characteristics that explain the ability of the muon to pass through specific materials (Ahlen et al., 1990). The exposure of the electromagnetic cascade/Extensive Air Showers (EAS) was a hot topic and has been performed by many researchers (Gaisser et al., 2016). The structure of this shower was experimentally investigated by using the technique of time distribution of measurement (Antoni et al., 2001).

Cosmic-ray muon interaction with metals exhibits an anomaly in the measured count rate behavior in relation to their depth. This is different from the interaction of gamma ray with metals, which shows intensity decrease represented by an exponential decay (Beer Lambert's law). In contrast, the measured intensity of the cosmic-ray muon shows an increase with the penetration length (Rossi Curve). The growth in the measured count rate is attributed to the particle and electromagnetic cascades (Bonolis, 2011; Goodkin,

1987; Heyland & Duncanson, 1953; Jánossy & Nagy, 1957; Khachatryan et al., 2010; Nagy, 1958; Rossi, 1964; Rossi et al., 1942; Swann & Ramsey, 1940). All these previous researches focused on the explanation rather than on counting the attenuation. The attenuation of cosmic-ray muons as a natural source with all continuous spectrum must be well understood to use it in applications. Thus, it is desirable that the attenuation of muon through materials is well described.

The unique nature of muon makes it the primary source used in Radiographic Imaging and Muography for large and dense objects (Borozdin et al., 2003; Procureur, 2017). Schultz et al. (Schultz et al., 2004) developed a simulation code and an algorithm to detect and discriminate the high-Z materials based on multiple scattering of cosmic-ray muons using Monte Carlo (MC) simulation and presented the validity of the detection for objects made of medium- and low-Z materials. Arteaga-Velázquez and his team (Arteaga-Velázquez et al., 2009) employed and developed MC simulation with another model and its initial collision, with the hadronic interaction model of EAS to study the performance of the experiment and the efficiency of the detector. MC Simulations based on Transport of Ions in Matter was performed by Autran et al., (2018) to investigate the detection of vertically-incident muons with an energy of 38 MeV. The MC simulation based on the hadronic interaction models

showed that the attenuation of the muon content of measured EAS in air is lower than that obtained from the experimental data (Antoni et al., 2001; Apel et al., 2017; Arteaga-Velázquez et al., 2009). Apel et al. (2017) reported that the discrepancy of the cosmic-ray muon absorption length is not yet clear and it could be better described. They suggested that modifications are required in certain models at high-energy interaction to resolve this discrepancy. If the absorption or attenuation length of muons in the atmosphere is complex, the situation becomes more complex in metals. In addition, all previous works focused on determining the energy loss or the differential cross-section by considering the particle and the electromagnetic cascades.

Relatively and recently, Braucher et al. (2013) proposed a new approach to determine the muon attenuation lengths from evolving cosmogenic nuclide concentrations along depth profiles below the Earth's surface. Apel et al. (2017) investigated the evolution of muon content to determine the attenuation length in the atmosphere using the experimental data obtained from the KASCADE-Grande observatory for energy of  $10^{16.3}$  and  $10^{17.0}$  eV. The effect of seasonal temperature variation on the muon intensity was studied by Grapes-3 experiment at high-energy (Arunbabu et al., 2017). A review of the different observational results of cosmic-ray muon showers and a presentation with emphasis on the interpretation, explanations, the diffusion, and magnetic lensing of air-shower physics have been reported by Mollerach & Roulet (2018). Schreiner (2016) theoretically and experimentally determined the attenuation coefficient values for aluminum and steel to study the tomography of large objects with low energy (110 MeV – 1.2 GeV) spectrum of muon using the GEANT (GEometry ANd Tracking) simulation software. Additionally, recent study by Altameemi et al. (2019) had also determined the attenuation coefficients for lead, copper, zinc, and aluminum using a very small solid angle to avoid incorrect measures because of the electromagnetic and particle cascade shower of muon. The calculations were performed by ignoring the growth part of the measured count rate graph and by curve-fitting the decreasing part with an exponential decay curve of measured count rate with thickness. The results obtained were also clearly different from the theoretical predictions made by the GEANT Simulation. The growth part in the measured count rate graph reflects the shower of photons and particles generated from the interaction of high-energy muons with the material. Such effect is supposed to occur even in the decay part and should therefore be considered. All in all, no work has considered the attenuation length in metals

and its anomaly of intensity in small thickness of layers yet.

Thus, this study aims to describe the intensity growth anomalous effect of the measured count rate in small thickness of metal layers by applied three methods. The attenuation coefficient of cosmic-ray muons was determined theoretically using these methods and the experimental data of cosmic-ray muons.

## 2. Methodology

This study started by proposing three methods to achieve the research aim and then determine the muon attenuation coefficient for metals theoretically using the previous experimental data (Altameemi et al., 2019). These experimental data were divided into three categories. The first one is the experimental values of the muon attenuation coefficient ( $\mu_{cp}$ ) for metal sheets of different types; lead (Pb), copper (Cu), zinc (Zn), and aluminum (Al) and with different thickness, 14 cm, 18.45 cm, 17.40 cm, and 20 cm, respectively. The second is the metals transition point ( $X_T$ ). The last one is the values of the maximum count rate ( $R_m$ ) and the initial count rate ( $R_0$ ) for each metal. All these data were adapted from previous study (Altameemi et al., 2019). The measurement was performed in a laboratory at the Department of Applied Physics, University Kebangsaan Malaysia, located at 101.78°E, 2.92°N, and 30 m above sea level. The radiation background of this place has been investigated previously (Samat & Evans, 2011; Tawalbeh et al., 2013) and has no effect on the current study. Two telescopes were used and each telescope consisted of two detectors (Altameemi & Gopir, 2016; Zain et al., 2010, 2009). The experimental setup allowed a very small solid angle of 0.05 sr. The efficiency of this experimental setup has already been investigated and statistically tested (Altameemi et al., 2019). The validity of data obtained using this experimental setup was verified by determining the transition points in the Rossi curves for the metal sheets (Altameemi et al., 2019, 2019).

When a beam of particles passes through a medium, its interaction is subject to the Beer–Lambert law, in which its intensity is exponentially reduced. This exponential form was used to fit the experimental data obtained for the measured intensity of cosmic-ray muons that penetrate the ground (Ahlen et al., 1990). The anomalous effect of the intensity ( $I$ )/count rate ( $R$ ) of the Rossi Curve can be described in this study by three methods beginning with the familiar equation of attenuation/Beer–Lambert law equation;  $R = R_0 e^{-\mu x}$ , where  $R$  is the measured count rate,  $R_0$  is the initial count rate when there is no layer of metal (thickness  $x = 0$ ),  $\mu$  is the muon attenuation coefficient and  $x$  is the total thickness of the metal.

## 2.1. Method A

The growth of the measured count rate is assumed to follow an exponential behavior with a growth coefficient  $\lambda$  and the decay with an attenuation coefficient  $\mu$ , which can be written as

$$\frac{dR}{dx} = -\mu R + \lambda R = (\lambda - \mu)R \quad (1)$$

The solution to this differential equation can be written in terms of the initial condition as

$$R = R_0 e^{(\lambda - \mu)x} \quad (2)$$

In the measured count rate graph or the Rossi curve, there is a peak called the transition point  $X_T$  at which the count rate stops growing and starts decaying. Equation (2) can be rewritten in terms of the maximum count rate  $R_m$  at this point and solved for  $(\lambda - \mu)$  as

$$(\lambda - \mu) = \frac{1}{X_T} \ln\left(\frac{R_m}{R_0}\right) \quad (3)$$

This equation shows that  $(\lambda - \mu)$  can be easily calculated using the Rossi curve obtained from the experimental data (Altameemi et al., 2019), when Eq. (3) is solved for  $R_0$  and substituted in Eq. (2), we obtain

$$R = R_m e^{(\lambda - \mu)|x - X_T|} \quad (4)$$

Therefore, Eq. (3) can be used to calculate  $(\lambda - \mu)$ , and then Eq. (4) can be fitted to the Rossi curve. The muon attenuation coefficient can be calculated after the growth coefficient is determined. The radiation length of these cascades has already been determined.

The radiation length is a characteristic of the material and is defined as the depth that retards the passing electron and loses 1/e (about 37%) of its energy. For cosmic-ray muons that propagate through the material, the radiation length ( $X_0$ ) is defined as the characteristic range for multiple scattering and other electromagnetic interactions (Schultz et al., 2004), the radiation length equation empirically calculated by Schultz et al. (2004):

$$X_0(\text{cm}) = \frac{716.4g/\text{cm}^2}{\rho} \frac{A}{Z(Z+1)\ln(287/\sqrt{Z})} \quad (5)$$

where  $Z$  and  $A$  are the atomic and mass numbers,  $\rho$  is mass density. Eq. (5) shows that the radiation length is reduced when a high- $Z$  material is used to attenuate the cosmic-ray muons. The experimental values of the radiation length of the material can also be used. This length is considered for all interactions caused by the penetrating muon, for the growth and the decay part, therefore it can be written as

$$(\lambda + \mu) = \frac{1}{X_0} \quad (6)$$

when Eq. (3) and Eq. (6) are simultaneously solved, we obtain

$$\mu(\text{cm}^{-1}) = \frac{1}{2X_0} - \frac{1}{2X_T} \ln\left(\frac{R_m}{R_0}\right) \quad (7)$$

Substituting Eq. (5) in Eq. (7), we obtain

$$\mu(\text{cm}^{-1}) = \frac{\rho Z(Z+1)\ln(287/\sqrt{Z})}{2A716.4g/\text{cm}^2} - \frac{1}{2X_T} \ln\left(\frac{R_m}{R_0}\right) \quad (8)$$

## 2.2. Method B

The change of the measured count rate with depth due to growth is not assumed to be constant  $\lambda$  as in Method A, but assumed to be proportional to  $(1/x)$

$$\frac{dR}{dx} = -\mu R + \frac{k}{x} R = \left(\frac{k}{x} - \mu\right) R \quad (9)$$

where  $k$  is a constant positive real number. When this equation is solved using the initial values of  $R = R_0$  at  $x = 0$ , we obtain

$$R = R_0 + R_0 x^k e^{-\mu x} \quad (10)$$

This equation can be used to obtain best fit for the Rossi curve by adjusting the parameters:  $k$  and  $\mu$ , to obtain the muon attenuation coefficient.

## 2.3. Method C

More considerations were taken into account to obtain a better description for the behavior of the measured muon count rate. The interaction between the muons with the material produces a shower of electron and photon cascades (Kampert & Watson, 2012). Therefore, it is important to distinguish between the cosmic-ray muon showers and the subsequent cascade showers in this method. The Method C count rate is assumed to implicitly and explicitly caused by the muons that interact with the material. Within a small particular thickness of material, the cascades penetrate and can then be detected as  $I_c$ , and the penetrating muons are explicitly measured as  $I_\mu$  mostly the same as  $I_{\mu 0}$  (the initial intensity of incident muons); the total intensity detected by the detector as events is the sum of these two intensities;  $I_d = I_{\mu 0} + I_c$ .

The muon passing through the absorber is assumed to produce a cascade of radiation each time it strikes every particle in the medium. The change of this cascade intensity or cascade count rate where ( $I_c \propto R_c$ ) with the distance between each collision  $s$  is assumed to have both growth and decay, and proportional to its intensity and exponential decay  $e^{(-vs)}$  with  $v$  is the attenuation coefficient of cascade, which can be written as

$$\frac{dR_c}{ds} = \lambda R_c e^{-vs} \quad (11)$$

where  $\lambda$  is a constant which considers as the cascade growth coefficient, the initial count rate  $R_{co}$  can be used when  $s = 0$  to obtain the constant of integration, hence Eq. (11) can be written as

$$R_c = R_{co} e^{\lambda(1-e^{-\mu s})} \quad (12)$$

The muon strikes many particles along its path through the material and causes many sources of cascades.  $R_{co}$  is supposed to be a function of the distance because it decreases while the muon penetrates deeper. Assuming that muon attenuation is subject to the Beer–Lambert law, it can be written as

$$R_{co} = \sum_{i=1}^N R_{co}(s_i) e^{-\mu s_i} \quad (13)$$

Since  $e^{-\mu s_i}$  describes the behavior of the muon attenuation with an attenuation coefficient  $\mu$  and assuming  $R_{co}(s_i) = R_{co}(s_0) = R_{\mu o}$  (equals to the muon count rate at  $s = 0$ ). The equation (13) can be rewritten in terms of  $x$  (the total thickness) instead of  $s$ , the sum over  $N$  collisions will be  $NR_{\mu o} e^{-\mu x}$ .  $N$  can be calculated by dividing the thickness with the free mean path of muon collections  $L_\mu = 1/\mu$ . Then  $N = \mu x$  and Eq. (12) can be rewritten as

$$R_c = R_{\mu o} \mu x e^{\lambda(1-e^{-\mu x}) - \mu x} \quad (14)$$

The total count rate penetrating the thickness of lead can be written as

$$R_d = R_{\mu o} + R_{\mu o} \mu x e^{\lambda(1-e^{-\mu x}) - \mu x} \quad (15)$$

The shower of the cascade spreads radially and its intensity is subject to the inverse square law as function of distance. The total intensity over a hemispherical area  $2\pi s^2$  is equal to a part of intensity of cascades that passes the front area of the detector  $A_d$ .  $F_A(s_i)$  is the radial irradiance correction factor for every collision of the muon. When the sum of  $F_A(s_i)$  is considered for every point source, it can be written as

$$\begin{aligned} F_A(x) &= \sum_{i=1}^{N+1} F_A(s_i) = \sum_{i=1}^{N+1} \frac{A_d}{2\pi s_i^2} = \frac{\mu^2 A_d}{2\pi} \sum_{i=1}^{N+1} \frac{1}{i^2} \\ &= \frac{\mu^2 A_d}{2\pi} \ln(N+1)^2 \end{aligned} \quad (16)$$

where  $N$  is the number of collisions between the muon particles and the particles of the medium of total thickness  $x$  and  $s_i = \Delta s_i$  with  $\Delta s = \frac{x}{N}$ ,  $N = \mu x$  and  $\mu = N/x$ , the radial irradiance correction factor in Eq. (16) can only be investigated after it is inserted in Eq. (15) for the cascade shower only as

$$R_d = R_{\mu o} + R_{\mu o} \frac{\mu^3 x A_d}{2\pi} \ln(\mu x + 1)^2 e^{\lambda(1-e^{-\mu x}) - \mu x} \quad (17)$$

It is important to note that inserting the irradiance factor may not be appropriate because the spreading of the shower over a hemispherical surface area has been observed. Therefore, two distinct theoretical

equations – one with the irradiance correction factor as in Eq. (17) and the other without the irradiance correction factor as in Eq. (15) may be used to describe the cascade shower effect in the Rossi curve.

The calculations of muon attenuation coefficient theoretically using the experimental data of measured count rates and based on the inclusion of the photon and particle cascades can be achieved using the three methods: A, B, and C. Method A was used for all metals, Pb, Cu, Zn, and Al when Method B and C were used for Pb only.

### 3. Results and discussion

The values of muon attenuation coefficients were obtained using Method A, which is based on Eq. (7), Method B which is based on fitting of Eq. (10) and Method C which is based on fitting of Eq. (15) and Eq. (17) to the experimental data.

#### 3.1. Method A

In Eq. (7), the radiation lengths ( $X_0$ ) can be calculated from Eq. (5) or taken directly from the tables of material properties, other parameters were taken from (Altameemi et al., 2019), see Table 1.

From Table 1,  $\mu_{cp}$  is the experimental attenuation coefficients for the metals (Altameemi et al., 2019), in which the exponentially decaying attenuation was assumed to start from the maximum point  $R_m$  at which the growth of measured count rate is halted. The results of the present work are shown with the columns' headings  $\mu_{c1}$ ,  $\mu_{c2}$ , and  $\mu_{c3}$ . The calculations following Method A have been presented in the previous section. To calculate  $\mu_{c1}$ , Eq. (7) and the data shown in Table 1 were used, as shown in Figure 1(a). When  $R_m$  was adjusted to  $19.55 \text{ s}^{-1} \cdot \text{sr}^{-1}$ , a ratio of  $R_m/R_o = 1.7$  was obtained for better fitting to the experimental data of lead, see Figure 1(b). This refined ratio of  $R_m/R_o = 1.7$  was used in Eq. (7) to calculate  $\mu_{c2}$ , which shows slight reduction in the values of the attenuation coefficient to  $0.72 \text{ cm}^{-1}$  as in Table 1. Since this fitting was exponential, it is convenient to use the obtained values in Table 1 ( $\mu_{cp}$ ) and to consider them in Method A,  $\mu_{cp} = \mu_{c3} - \lambda$  to include the growth effect and calculate  $\mu_{c3}$  from;

$$\mu_{c3} (\text{cm}^{-1}) = \frac{1}{2X_0} + \frac{\mu_{cp}}{2} \quad (18)$$

**Table 1.** The muon attenuation coefficients ( $\mu_{c1}$ ,  $\mu_{c2}$  and  $\mu_{c3}$ ) for Pb, Cu, Zn, and Al from Method A.

M	$X_T$ (cm)	$\mu_{cp}$ ( $\text{cm}^{-1}$ )	$R_m/R_o$	$X_0$ (cm)	$\mu_{c1}$ ( $\text{cm}^{-1}$ )	$\mu_{c2}$ ( $\text{cm}^{-1}$ )	$\mu_{c3}$ ( $\text{cm}^{-1}$ )
Pb	1.50	0.15	1.526	0.56	0.752	0.716	0.968
Cu	3.00	0.07	1.534	1.44	0.276	0.259	0.382
Zn	4.00	0.06	1.431	1.74	0.243	0.221	0.317
Al	9.00	0.05	1.343	8.90	0.039	0.027	0.081



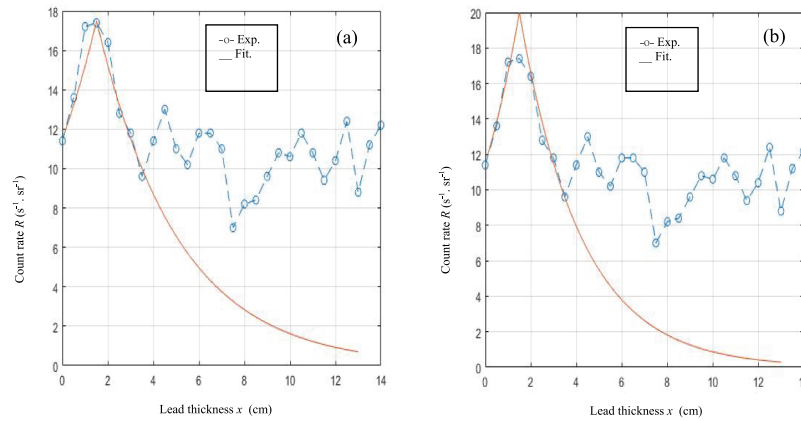


**Figure 1.** The muon count rate  $R$ , versus the lead thickness  $x$ , of Method A, based on (a) fitting of Eq. (7) and (b) adjusted fitting with higher  $R_m$ .

The muon attenuation coefficient obtained from Eq. (18) showed slight increase in the values as in Table 1. By the same way, the attenuation coefficients of the other elements are calculated. Therefore, the differences between these three values are attributed to the quality of the fit; however, they are all based on theoretical calculation using Method A.

There was only one previous work that attempted to obtain the theoretical values of the muon attenuation coefficient for Al using the GEANT simulation software the theoretical value was ( $0.039 \text{ cm}^{-1}$ ) and experimentally ( $0.0988 \text{ cm}^{-1}$ ), for steel with values of  $0.03078$  and  $0.125 \text{ cm}^{-1}$ , respectively (Schreiner, 2016). Our results for Al (in Table 1) agreed with the theoretical values (Schreiner, 2016) more than that obtained by measurement. The trend of the muon attenuation length with the atomic number reflects the ability of the material to stop the high-energy cosmic muons. As seen from the table, the muon attenuation length increases for materials with higher atomic number. Eq. (8) shows this nonlinear behavior.

### 3.2. Method B

Two parameters  $k$  and  $\mu$  were adjusted to obtain best fit with the experimental data of lead. Three values of  $k$  were chosen:  $-1$ ,  $1$ , and  $2$ , with each  $\mu$  value was adjusted to obtain the best fit. Our results show that when  $k = -1$ , no reasonable fit was obtained with any value of  $\mu$ . On the other hand, when  $k = 1$ , the attenuation coefficient obtained was very close to the value obtained using Method A as shown in Figure 2(a). A value of  $\mu > 1$  was needed to have the best fit with  $k = 2$  see Figure 2(b). Therefore, the most appropriate fit is when  $k = 1$ , and the theoretical equation that describes the muon count rate as a function of thickness is

$$R = R_0 + R_0 x e^{-\mu x} \quad (19)$$

In accordance with Eq. (19) in Method B,  $k$  is a growth parameter and is meant to be positive. When the fit confirms its value  $= 1$ , this good coincidence may reflect the inverse proportionality of the muon attenuation to the depth of material (lead) as in Eq. (19). Therefore, the results obtained using Method B agree with the value of muon attenuation coefficient in lead ( $\sim 0.8 \text{ cm}^{-1}$ ) obtained using Method A.

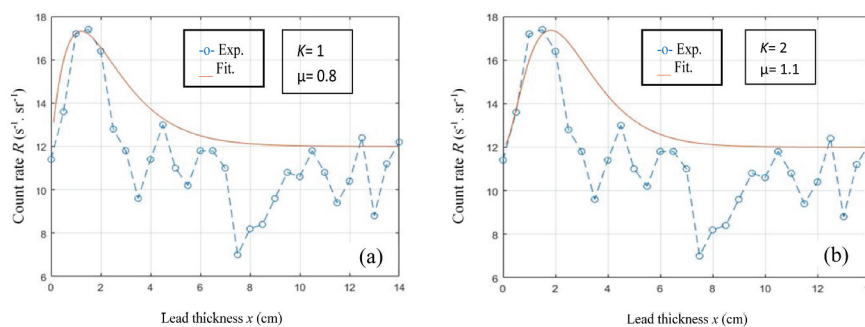


**Figure 2.** The muon count rate  $R$ , versus the lead thickness  $x$ , of Method B, based on fitting of Eq. (10), where (a)  $K = 1$  and (b)  $K = 2$ .

### 3.3. Method C

The growth and attenuation of muons in the materials were assumed to be caused by the electromagnetic cascade and most fast-moving muons easily penetrated the lead layers. The difference between Eq. (15) and Eq. (17) is the inclusion of the radial irradiance correction in the cascade intensity in Eq. (17). When Eq. (15) was used to calculate  $R_{di}$ ,  $R_{\mu o}$  was taken from the experimental measurement to be equal to  $11.4 \text{ s}^{-1} \cdot \text{sr}^{-1}$ . The cascade attenuation coefficient  $\nu$  was taken from the radiation length of photon-electron cascade  $L_o = 6.37 \text{ g/cm}^2$  (Groom & Klein, 2000) to be calculated using  $\nu = \rho/L_o$ , where  $\rho$  is the mass density of lead. The muon attenuation  $\mu$  and the cascade growth coefficient  $\lambda$  are adjusted to obtain the best fit. Figure 3 shows the values.

When Eq. (17) was used to obtain a good fit, different values of  $\mu$  and  $\lambda$  were chosen to find the effect of each on the behavior of the curve as in the fitting of Eq. (15). The best fit was obtained with  $\mu = 1.6 \text{ cm}^{-1}$ ,  $\lambda = 2.5 \text{ cm}^{-1}$  and  $\nu = 1.78 \text{ cm}^{-1}$  as shown in Figure 4 (d). The muon attenuation factor obtained from Eq. (17) describes the count rate better than that obtained from Eq. (15) for fitting. Equations (15) and (17) describe the count rate of muon events in lead layers well because in both cases, the variation in the intensity of electron-photon cascade with depth grows linearly (with a factor  $\lambda$ ) and subsequently decays exponentially (with  $\nu$  coefficient). This supports the proposed hypothesis that multiple points of cascade sources exist along the path of muon in the lead layers. Since Eq. (17) describes the experimental count rate better than Eq. (15), this implies that the assumption of

radial irradiance from multiple points of cascade sources is valid.

The values of the muon attenuation factor for lead obtained from the two Methods (A and B) showed good agreement  $\mu = 0.8 \text{ cm}^{-1}$ . The attenuation of muon from Method C was about  $\mu = 1.2\text{--}1.6 \text{ cm}^{-1}$ , which is greater than that obtained from Methods A and B.

Although the general shape of Rossi's Curve has been explained previously, the reason for the formation of the Rossi Curve peak is still unexplained, because there is no evidence whether this peak is totally formed due to the muons or particular muons (muon with electromagnetic particles) within the continuous spectrum. It can neither be confirmed also, whether this peak is produced by low- or high-energy muons as a result of the possibility of more than one peak that has been observed earlier; further investigation is therefore desirable for other metals, elements, and alloys.

### 4. Conclusion

Three methods, A, B, and C, were proposed by the researchers in this study to describe the anomalous increase of muon intensity in small metal thicknesses. The muon attenuation coefficients in lead, copper, zinc, and aluminum were calculated using Method A with the experimental data of count rate event detection in relation to the thickness of metals. A new theoretical formula for the muon attenuation coefficient in terms of mass density, atomic, and mass number is thus presented. The value for aluminum agrees with previous theoretical calculation. The values for lead obtained from the

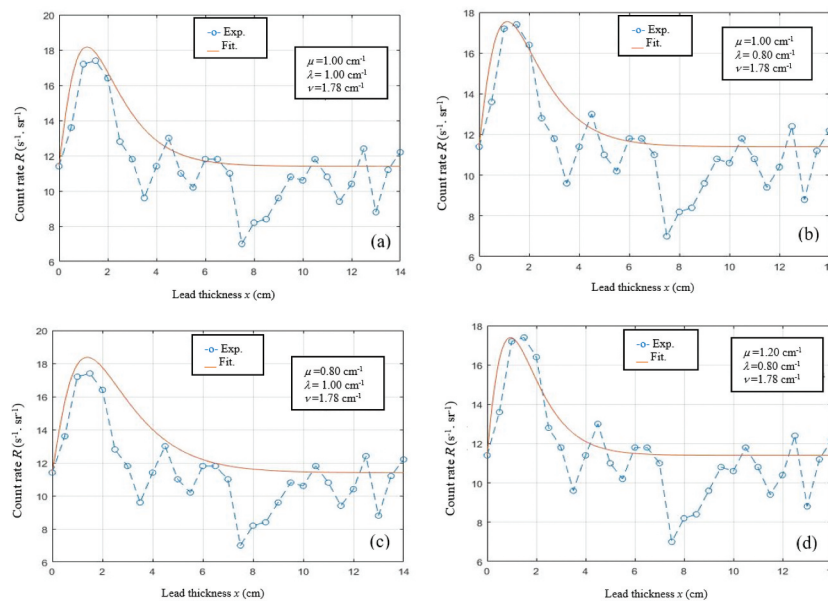
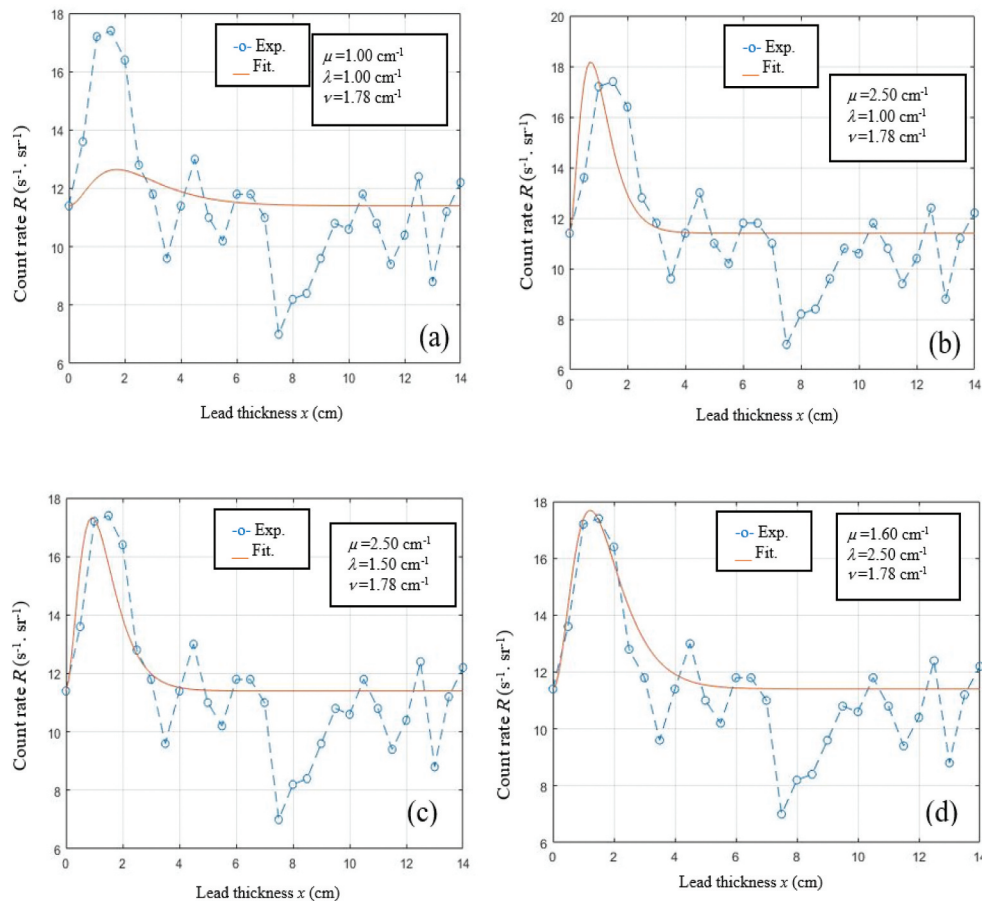


Figure 3. The muon count rate  $R$ , versus the lead thickness  $x$ , of Method C, based on fitting of Eq. (15). For different values of  $\mu$  and  $\lambda$ .



**Figure 4.** The muon count rate  $R$ , versus the lead thickness  $x$ , of Method C, based on fitting of Eq. (17), for different values of  $\mu$  and  $\lambda$ . best fitting in (d).

two methods (A and B) showed good agreement. Method B and C were proposed only for lead to determine the muon attenuation coefficient theoretically. Based on Method C, the growth and the decay in the cosmic muon count rates were well described when the muon was assumed to produce multiple points of cascade sources from every collision along its path through the materials. However, the attenuation of muon was implicitly determined and the value was about  $1.2 - 1.6 \text{ cm}^{-1}$ , which is greater than that from Methods A and B. The muon attenuation coefficient can be determined using theoretical calculations, and more work is desired to develop and enhance the description of the cosmic muon intensity attenuation. The values of results obtained could be a good reference for anisotropic muon attenuation coefficients for muography studies.

## Acknowledgments

We would like to acknowledge the Department of Applied Physics, Faculty of Science and Technology, Universiti Kebangsaan Malaysia for provided the

laboratory space to conduct our observations.


## Disclosure statement

No potential conflict of interest was reported by the authors.

## ORCID

Rasha N. I. Altameemi  <http://orcid.org/0000-0002-5461-9576>

Nurul Shazana Abdul Hamid  <http://orcid.org/0000-0002-8674-5921>

Wan Mohd Aimran Wan Mohd Kamil  <http://orcid.org/0000-0001-6875-4288>

Saad M. Saleh Ahmed  <http://orcid.org/0000-0003-4871-3731>

## References

- Ahlen, S. P., Ambrosio, M., Auriemma, G., Baldini, A., Barbarino, G. C., Barish, B., Battistoni, G., Bellotti, R., Bemporad, C., Bernardini, P., Bilokon, H., Bisi, V., Bloise, C., Bower, C., Cafagna, F., Calicchio, M., Campana, P., Chiarella, W., Chrysicopoulou, P., Worstell, W., & Worstell, S. (1990). Study of penetrating cosmic ray muons and search for large scale anisotropies at the Gran Sasso Laboratory.

- Physics Letters B*, 249(1), 149–156. [https://doi.org/10.1016/0370-2693\(90\)90541-D](https://doi.org/10.1016/0370-2693(90)90541-D)
- Altameemi, R. N. I., Hamid, N. S. A., Kamil, W. M. A. W. M., & Ahmed, S. M. S. (In-Press). Examination the cosmic ray muon attenuation by heavy metal alloys. *ICeSSAT Conference Proceedings*, Johor, Malaysia.
- Altameemi, R. N. I., & Gopir, G. (2016). Effect of copper and aluminium on the event rate of cosmic ray muons at ground level in Bangi, Malaysia. *AIP Conference Proceedings*, 040005.
- Altameemi, R. N. I., Hamid, N. S. A., Kamil, W. M. A. W. M., & Ahmed, S. M. S. (2019). Determination of muon absorption coefficients in heavy metal elements. *Journal of Radiation Research and Applied Sciences*, 12(1), 1,281–288. <https://doi.org/10.1080/16878507.2019.1652965>
- Altameemi, R. N. I., Hamid, N. S. A., Kamil, W. M. A. W. M., Ahmed, S. M. S., & Gopir, G. (2019). Investigation of simple portable telescope validity for muon detection inside metals. *Sains Malaysiana*, 48, 377–383. <https://doi.org/10.17576/jsm-2019-4802-15>
- Antoni, T., Apel, W. D., Badea, A. F., Bekk, K., Bernlöhner, K., Blümer, H., Bollmann, E., Bozdog, H., Brancus, I. M., Chilingarian, A., Daumiller, K., Doll, P., Engler, J., Feßler, F., Gils, H. J., Glasstetter, R., Haeusler, R., Haungs, S., Heck, D., Zagromski, S., & Zagromski, W. (2001). Time structure of the extensive air shower muon component measured by the KASCADE experiment. *Astroparticle Physics*, 15(2), 149–165. [https://doi.org/10.1016/S0927-6505\(00\)00148-1](https://doi.org/10.1016/S0927-6505(00)00148-1)
- Apel, W. D., Arteaga-Velázquez, J. C., Bekk, K., Bertaina, M., Blümer, J., Bozdog, H., Brancus, I. M., Cantoni, E., Chiavassa, A., Cossavella, F., Daumiller, K., de Souza, V., Di Pierro, F., Doll, P., Engel, R., Fuhrmann, D., Gherghel-Lascu, A., Zabierowski, J., Glasstetter, R., Grupen, C., & Zabierowski, J. (2017). Probing the evolution of the EAS muon content in the atmosphere with KASCADE-Grande. *Astroparticle Physics*, 95, 25–43. <https://doi.org/10.1016/j.astropartphys.2017.07.001>
- Arteaga-Velázquez, J. C., Apel, W. D., Badea, F., Bekk, K., Bertaina, M. E., Blümer, J., Bozdog, H., Brancus, I., Brüggemann, M., Buchholz, P., Cantoni, E., Chiavassa, A., Cossavella, F., Daumiller, K., de Souza, V., Di Pierro, F., Doll, P. J., Engler, J., Finger, M., Zabierowski, J., & Zabierowski, R. (2009). The constant intensity cut method applied to the KASCADE-Grande muon data. *Nuclear Physics B - Proceedings Supplements*, 196, 183–186. <https://doi.org/10.1016/j.nuclphysbps.2009.09.033>
- Arunbabu, K. P., Ahmad, S., Chandra, A., Dugad, S. R., Gupta, S. K., Hariharan, B., Hayashi, Y., Jagadeesan, P., Jain, A., Jhansi, V. B., Kawakami, S., Kojima, H., Mohanty, P. K., Morris, S. D., Nayak, P. K., Oshima, A., Rao, B. S., Reddy, L. V., Shibata, S., Tanaka, K., & Zuberi, M. (2017). Dependence of the muon intensity on the atmospheric temperature measured by the GRAPES-3 experiment. *Astroparticle Physics*, 94, 22–28. <https://doi.org/10.1016/j.astropartphys.2017.07.002>
- Autran, J. L., Munteanu, D., Saoud, T. S., & Moindjie, S. (2018, June). Characterization of atmospheric muons at sea level using a cosmic ray telescope. *Nuclear Instruments and Methods in Physics Research Section A: Accelerators, Spectrometers, Detectors and Associated Equipment*, 903, 77–84. <https://doi.org/10.1016/j.nima.2018.06.038>
- Bonolis, L. (2011). Walther Bothe and Bruno Rossi: The birth and development of coincidence methods in cosmic-ray physics. *American Journal of Physics*, 79, 1133–1150.
- Borozdin, K. N., Hogan, G. E., Morris, C., Priedhorsky, W. C., Saunders, A., Schultz, L. J., & Teasdale, M. E. (2003). Surveillance: Radiographic imaging with cosmic-ray muons. *Nature*, 422, 277–278. <https://doi.org/10.1038/422277a>
- Braucher, R., Bourlès, D., Merchel, S., Romani, J. R. V., Fernandez-Mosquera, D., Marti, K., Leanni, L., Chauvet, F., Arnold, M., Aumaitre, G., & Keddadouche, K. (2013). Determination of muon attenuation lengths in depth profiles from in situ produced cosmogenic nuclides. *Nucl. Instruments Methods Phys. Res. Sect. B Beam Interact. With Mater. Atoms*, 294, 484–490. <https://doi.org/10.1016/j.nimb.2012.05.023>
- Gaisser, T. K., Engel, R., & Resconi, E. (2016). *Cosmic rays and particle physics*. Cambridge University Press.
- Goodkin, R. J. (1987). (2005) Historical Introduction. In: *Astroparticle Physics*. Springer, Berlin, Heidelberg. [https://doi.org/10.1007/3-540-27670-X\\_1](https://doi.org/10.1007/3-540-27670-X_1)
- Groom, D. E., & Klein, S. R. (2000). Passage of particles through matter. *The European Physical Journal C*, 15, 163–173. <https://doi.org/10.1007/BF02683419>
- Heyland, G. R., & Duncanson, W. E. (1953). A search for irregularities in the absorption of cosmic rays in lead. *Proceedings of the Physical Society - Section A*, 66(1), 33. <https://doi.org/10.1088/0370-1298/66/1/306>
- PDG) Particle Data Group. 2015. <http://pdg.lbl.gov/2015/AtomicNuclearProperties/>
- Jánossy, L., & Nagy, L. (1957). Experiments on the Rossi curve. *Acta Physica Academiae Scientiarum Hungaricae*, 6(3), 467. <https://doi.org/10.1007/BF03156617>
- Kampert, K., & Watson, A. A. (2012). Extensive air showers and ultra high-energy cosmic rays: A historical review. *The European Physical Journal H*, 37(3), 359–412. <https://doi.org/10.1140/epjh/e2012-30013-x>
- Khachatryan, V., Sirunyan, A. M., Tumasyan, A., Adam, W., Bergauer, T., Dragicevic, M., Erö, J., Fabjan, C., Friedl, M., Frühwirth, R., Ghete, V. M., Hammer, J., Häseler, S., Hoch, M., Hörmann, N., Hrubec, J., Jeitler, M., & Weinberg, M. (2010). Measurement of the charge ratio of atmospheric muons with the CMS detector. *Physics Letters, Section B: Nuclear, Elementary Particle and High-Energy Physics*, 692(2), 83–104. <https://doi.org/10.1016/j.physletb.2010.07.033>
- Mollerach, S., & Roulet, E. (2018). Progress in high-energy cosmic ray physics. *Progress in Particle and Nuclear Physics*, 98, 85–118. <https://doi.org/10.1016/j.ppnp.2017.10.002>
- Nagy, L. (1958). Shower production at small thicknesses of absorber. *Acta Physica Academiae Scientiarum Hungaricae*, 9(1), 63–72. <https://doi.org/10.1007/BF03157272>
- Procureur, S. (2017). Muon imaging: Principles, technologies and applications. *Nuclear Instruments and Methods in Physics Research Section A: Accelerators, Spectrometers, Detectors and Associated Equipment*, 878, 169–179. <https://doi.org/10.1016/j.nima.2017.08.004>
- Rossi, B. (1964). *Cosmic rays*. McGraw-Hill.
- Rossi, B., Greisen, K., & Exel, R. U. Y. (1942). Origin of the soft component of cosmic rays. *Physical Review*, 61(3–4), 121. <https://doi.org/10.1103/PhysRev.61.121>
- Samat, S. B., & Evans, C. J. (2011). Determination of radiation hazard arising from the 40K content of bottled mineral water in Malaysia. *Sains Malaysiana*, 40(12), 1355–1358.
- Schreiner, H. F., III. (2016). *Methods and simulations of muon tomography and reconstruction*. The University of Texas at Austin. <http://hdl.handle.net/2152/39757>
- Schultz, L. J., Borozdin, K. N., Gomez, J. J., Hogan, G. E., McGill, J. A., Morris, C. L., Priedhorsky, W. C., Saunders, A., & Teasdale, M. E. (2004). Image reconstruction and material Z discrimination via cosmic ray muon radiography. *Nuclear Instruments and Methods in Physics Research Section A: Accelerators, Spectrometers, Detectors and Associated Equipment*, 519(3), 687–694. <https://doi.org/10.1016/j.nima.2003.11.035>
- Stanev, T. (2010). *High energy cosmic rays*. Springer.
- Swann, W. F. G., & Ramsey, W. E. (1940). The secondary peak in the Rossi curve for tin. *Physical Review*, 477, 661–663. <https://doi.org/10.1103/PhysRev.58.477>



- Tawalbeh, A. A., Samat, S. B., & Yasir, M. S. (2013). Radionuclides level and its radiation hazard index in some drinks consumed in the central zone of Malaysia. *Sains Malaysiana*, 42(3), 319–323.
- Zain, N. M., Gopir, G. K., Yatim, B., Sanusi, H., & Husain, N. H. (2009). Zenith angle dependence of muon rate at ground level in Bangi. In *2009 International Conference on Space Science and Communication, IconSpace - Proceedings*, Johar, Malaysia (pp. 191–194). [5352639]. <https://doi.org/10.1109/ICONSPACE.2009.5352639>
- Zain, N. M., Gopir, G. K., Yatim, B., Sanusi, H., & Husain, N. H. (2010). Observation of ground level Muon at Bangi in 2008-2009. *AIP Conference Proceedings*, 1250(1), 468–471. <https://doi.org/10.1063/1.3469710>